

OpenFly: A Comprehensive Platform for Aerial Vision-Language Navigation

Yunpeng Gao^{1,2*}, Chenhui Li^{1*}, Zhongrui You^{1,3*}, Junli Liu^{1,2*}, Zhen Li^{1,4*}, Pengan CHEN^{1,5}, Qizhi Chen^{1,6}, Zhonghan Tang^{1,7}, Liansheng Wang¹, Penghui Yang^{1,8}, Yiwen Tang^{1,2}, Yuhang Tang^{1,2}, Shuai Liang^{1,9}, Songyi Zhu¹, Ziqin Xiong^{1,4}, Yifei Su^{1,10}, Xinyi Ye¹, Jianan Li¹, Yan Ding¹, Dong Wang¹, Zhigang Wang^{1†}, Bin Zhao^{1,2†}, Xuelong Li^{1,11}

¹Shanghai AI Laboratory, ²Northwestern Polytechnical University,

³Beijing University of Posts and Telecommunications, ⁴Shanghai Jiao Tong University,

⁵The University of Hong Kong, ⁶Zhejiang University,

⁷University of Science and Technology of China,

⁸East China University of Science and Technology, ⁹Fudan University,

¹⁰Institute of Automation, Chinese Academy of Sciences, ¹¹TeleAI

*Equal Contribution, †Corresponding Author

<https://shailab-ipec.github.io/openfly/>



Figure 1: Overview of OpenFly. This work consists of the integration of 4 rendering engines, an automatic toolchain for data generation, a large-scale aerial VLN dataset comprising 100K trajectories and instructions, and a keyframe-aware VLN model emphasizing key observations.

Abstract:

Vision-Language Navigation (VLN) aims to guide agents by leveraging language instructions and visual cues, playing a pivotal role in embodied AI. Indoor VLN has been extensively studied, whereas outdoor aerial VLN remains underexplored. The potential reason is that outdoor aerial view encompasses vast areas, making data collection more challenging, which results in a lack of benchmarks. To address this problem, we propose **OpenFly**, a platform comprising various rendering engines, a versatile toolchain, and a large-scale benchmark for aerial VLN. Firstly, we integrate diverse rendering engines and advanced techniques for environment simulation, including Unreal Engine, GTA V, Google Earth, and 3D Gaussian Splatting (3D GS). Particularly, 3D GS supports real-to-sim rendering, further enhancing the realism of our environments. Secondly, we develop a highly automated toolchain for aerial VLN data collection, streamlining point cloud acquisition, scene semantic segmentation, flight trajectory creation, and instruction generation. Thirdly, based on the toolchain, we construct a large-scale

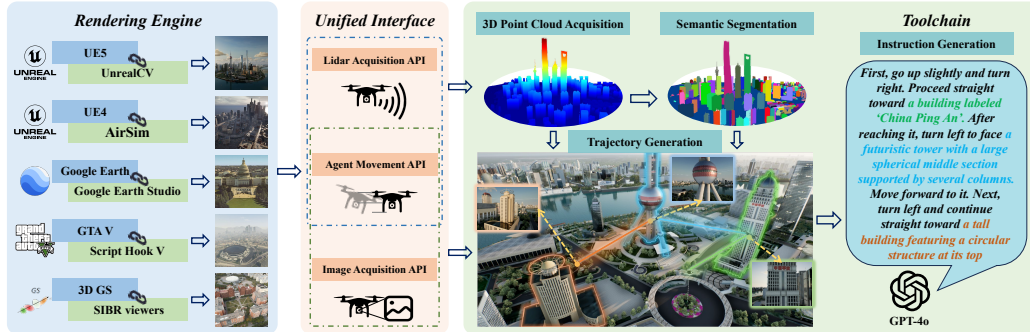


Figure 2: Framework of the automatic data generation. Various rendering engines are first integrated, providing diverse high-quality scenes. Built on these, several interfaces and tools are developed, enabling automated generation of trajectories and instructions.

aerial VLN dataset with 100k trajectories, covering diverse heights and lengths across 18 scenes. Moreover, we propose OpenFly-Agent, a keyframe-aware VLN model emphasizing key observations during flight. For benchmarking, extensive experiments and analyses are conducted, evaluating several recent VLN methods and showcasing the superiority of our OpenFly platform and agent. The toolchain, dataset, and codes will be open-sourced.

Keywords: Aerial Vision-Language Navigation (VLN), benchmark, toolchain

1 Introduction

Embodied AI has drawn increasing research interest, where vision-language navigation (VLN) is a key task, aiming to navigate agents to a target location according to linguistic instructions and visual observations. Recently, many VLN datasets have been established, *e.g.*, TouchDown [1], REVERIE [2], R2R [3], RxR [4], CVDN [5], VLN-CE [6], and LANI [7], which significantly facilitate a series of VLN methods [8, 9, 10, 11, 12, 13, 14, 15, 16]. However, all these works focus on indoor or ground-based agents, overlooking unmanned aerial vehicles (UAVs) that play an important role in aerial photography, rescue operations, and cargo transportation.

Most recently, AerialVLN [17] and OpenUAV [18] have made significant strides by leveraging UAV simulators to bridge gaps in aerial VLN datasets, thus greatly advancing the development of this field. However, several challenges remain that need to be addressed:

- **Insufficient data diversity.** Existing methods rely on AirSim and Unreal Engine (UE) to control UAVs, limiting them to digital assets compatible with these platforms, reducing the diversity of available data and restricting the potential use of more photorealistic sources.
- **Inefficient data collection.** The process of generating trajectories relies on pilots operating UAVs in simulators, followed by manual annotation to create language instructions. The entire process is labor-intensive, time-consuming, and difficult to scale.
- **Inadequate data scale.** Current datasets for aerial VLN remain relatively small, with only around 10k trajectories, which is far behind embodied manipulation datasets. For example, Open X-Embodiment [19] has collected 1M episodes of manipulation data, which has significantly accelerated the development of vision-language-action (VLA) models.

To address these issues, we propose **OpenFly**, a comprehensive platform consisting of diverse rendering engines, a versatile toolchain, and a large-scale benchmark for the aerial VLN task. **To enhance data diversity**, the platform is established on various widely-used rendering engines and

advanced techniques, *i.e.*, UE, GTA V, Google Earth, and 3D Gaussian Splatting (3D GS), enabling us to utilize a wide range of assets as shown in Fig. 1. In particular, we use UAVs to capture numerous real-world images and integrate 3D GS technology into our platform to reconstruct realistic 3D scenes, empowering real-to-sim simulation. **To improve the efficiency of data collection**, we develop a versatile toolchain for automated aerial VLN data generation as depicted in Fig. 2. Specifically, point cloud acquisition is first conducted to capture the 3D occupancy of a scene. Next, scene semantic segmentation is performed to identify and select landmarks as waypoints along the flight trajectories. Building on these tools, trajectory generation is then carried out, taking landmarks and point clouds as input, using predefined flight actions as basic units, and automatically searching for a collision-free trajectory. Finally, we feed the trajectories and corresponding UAV-egocentric images into a vision-language-model (VLM), *i.e.*, GPT-4o, to generate linguistic instructions. The entire pipeline is highly automated, reducing the reliance on UAV pilots and annotators. **To collect a large-scale dataset**, we meticulously collected 18 high-quality scenes, generating various trajectories of differing heights and lengths. Benefitting from our toolchain, we are able to quickly construct a dataset of **100k** samples, significantly larger than existing datasets.

Besides, we propose **OpenFly-Agent**, a keyframe-aware aerial VLN model incorporating an adaptive frame-level sampling mechanism to emphasize critical observations. Note that this keyframe sampling mechanism is crucial for the visual encoding of aerial VLN, as UAVs fly quickly and observations change rapidly. Extensive experiments are conducted on the OpenFly dataset to evaluate numerous methods, establishing a comprehensive benchmark for the aerial VLN tasks. Overall, our contributions can be summarized as follows:

- We build OpenFly on multiple rendering engines and develop a versatile toolchain, enabling the automatic generation of data with both great diversity and efficiency.
- We have constructed a novel aerial VLN benchmark comprising **100k** trajectories across 18 high-quality scenes. To the best of our knowledge, this is the largest aerial VLN benchmark to date, and users can collect more customized data using the OpenFly platform.
- We propose OpenFly-Agent, a keyframe-aware VLN model. Extensive experiments demonstrate its superior performance compared to other methods.

2 Related Works

2.1 Vision-Language Navigation Datasets

Numerous datasets have been proposed to accelerate the VLN task. R2R [3] focuses on evaluating agents in unseen buildings and provides discrete navigation options. RxR [4] provides a more densely annotated VLN dataset. TouchDown [1] and REVERIE [2] have each contributed a dataset from real-life environments, which requires a ground-based agent to follow instructions and find a target object. CVDN [5] presents a cooperative VLN dataset where agents can access the history of human cooperation for inference. All the above datasets are graph-based, where navigable points are predefined. LANI [7] and VLN-CE [6] propose the VLN task in continuous outdoor/indoor environments, enabling agents to move freely to any unobstructed point. Recently, a few works have tried to construct VLN datasets for aerial space. ANDH [20] establishes a dialogue-based aerial VLN dataset with bird-view images. CityNav [21] builds on the point cloud data from SensatUrban [22] and linguistic annotations from CityRefer [23], which requires a real-world 2D map to help locate specific landmarks in the instruction. AerialVLN [17] and OpenUAV [18] integrate AirSim and UE to create VLN scenes where pilots can control UAVs to generate various trajectories.

2.2 Vision-Language Navigation Methods

VLN methods require agents to understand and complete language instructions according to visual observations. In graph-based works [24, 25, 26, 27], agents move among predefined graph nodes.

Recently, LLM-driven works [28, 29, 30, 31] use the reasoning ability of large language models to infer the next node. Although great progress has been achieved, these methods are not applicable in real unknown environments. In contrast, [32, 33, 34, 16] explore VLN in continuous environments for more realistic applications. More recently, a few works attempt to address the problem of aerial VLN based on UAVs, among which AerialVLN [17] proposes a lookahead guidance method to generate more reasonable ground-truth trajectories during training. STMR [35] designs a matrix representation to improve the spatial reasoning of LLMs. OpenUAV [18] incorporates extra human assistance aligned with the ground truth (GT) trajectory to guide the navigation.

3 Automatic Data Generation

In this section, we first describe several rendering engines and data resources, then present the developed toolchain. The whole automatic data generation framework is illustrated in Fig. 2.

3.1 Rendering Engines and Data Resources

Unreal Engine. UE is a rendering engine capable of providing highly realistic virtual environments. We meticulously select 8 urban scenes, covering more than $100km^2$ areas. These scenes include a variety of assets such as buildings, streets, traffic lights, vehicles, and pedestrians, encompassing a wide range of architectural styles.

GTA V. GTA V is an open-world game that is frequently used by researchers due to its highly realistic environment. The game features a meticulously crafted cityscape modeled after Los Angeles, encompassing various buildings and locations such as skyscrapers, gas stations, parks, and plazas.

Google Earth. Google Earth is a virtual globe software, which builds a 3D earth model by integrating satellite imagery and aerial photographs. From this engine, we select four urban scenes covering a total area of $53.60km^2$, *i.e.*, Berkeley, Osaka, Washington, D.C., and St. Louis.

3D Gaussian Splatting. 3D GS excels in realistic scene reconstruction by capturing intricate textures. It enables the creation of highly detailed, lifelike virtual environments, significantly improving the realism of digital scenes. Due to these features, we use a hierarchical 3D GS method [36] to reconstruct and render multiple real scenes. Practically, we gathered data from five campuses across three universities using UAVs. These campus scenes include various types and styles of landmarks, such as libraries, bell towers, waterways, lakes, playgrounds, construction sites, and lawns. **More details of rendering engines, data resources, and examples can be found in Appendix A.**

3.2 Toolchain for Automatic Data Collection

To achieve automatic data generation, we first integrate the above rendering engines and design three unified interfaces to control the agent movement and acquire sensor data (presented in Appendix C). Based on these interfaces, we further develop a toolchain, streamlining point cloud acquisition, scene semantic segmentation, trajectory creation, and instruction generation.

3D Point Cloud Acquisition. Our OpenFly provides two methods to reconstruct the point cloud map for different scenes. 1) Rasterized Sampling Reconstruction: For UE and GTA V scenes, we customize rasterized sampling points at appropriate resolutions, and then use the developed interface to obtain the local point cloud at the sampling points and stitch them for the entire scene. 2) Image-Based Sparse Reconstruction: In 3D GS, the scene reconstruction process begins with the open-source COLMAP [37] framework, which generates a sparse point cloud from input images. We directly export and use the point clouds obtained from this step.

Scene Semantic Segmentation. VLN requires meaningful landmarks as navigation targets. Thus, we offer three semantic segmentation methods to identify landmarks. 1) 3D Scene Understanding: A sequence of top-down views of the scene is captured in a rasterized format, followed by the off-the-shelf Octree-Graph [38] to extract semantic 3D instances. 2) Point Cloud Projection and Contour Extraction: We acquire the point cloud of a scene and project the voxelized point cloud onto the

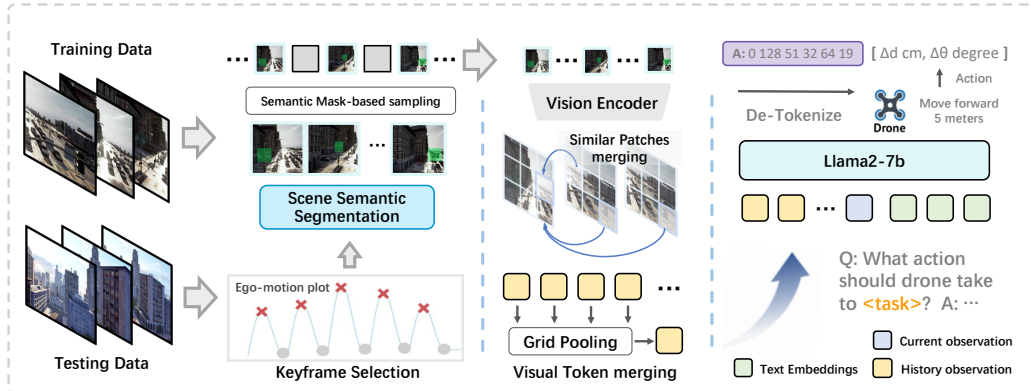


Figure 4: The architecture of OpenFly-Agent. Keyframes at the time of action transitions are selected to extract crucial observations as the history, with corresponding visual tokens compressed to reduce the computational burden.

Therefore, we set different trajectory lengths and flight heights to obtain rich data. Fig. 3a exhibits the distribution of these data, with their lengths ranging from 0 to 300 meters, and the heights ranging from 0 to 150 meters. Notably, we follow the mainstream methods [6, 17] to use discrete actions, *e.g.*, ‘Forward’ and ‘Turn left’, for trajectory generation, where the step size is 3m for ‘Forward’ action, making its proportion much higher than that of ‘Turn’ and altitude adjustments. This highly unbalanced action distribution might cause the VLN model to overfit the dominant action. To alleviate this problem, we employ three granularities of ‘Forward’ action during trajectory generation, *i.e.*, 3m, 6m, and 9m. Fig. 3b presents the action distribution of our dataset. It should be noted that the OpenFly platform also supports trajectory generation with continuous waypoints.

For instruction analysis, the vocabulary size of our dataset is 15.6K, and the average length of instructions is 59. Fig. 3c and Fig. 3d illustrate the word clouds of nouns and verbs, where ‘building’, ‘windows’, and ‘skyscraper’ are the most common references, and ‘proceed’ and ‘turn’ are the mostly used verbs for VLN. Due to the space limitation, **we put more details of our dataset and other ones as well as more instruction analyses in Appendix H.**

4.2 Dataset Split

Similar to previous works, we divide the dataset into three splits, *i.e.*, *Train*, *Test Seen*, *Test Unseen*. For the *Train* split, 7 scenes under the UE rendering engine account for 75.7% of all data, since UE provides the largest number of scenes, where different amounts of trajectories are sampled according to the areas of scenes. The 4 scenes created by 3D GS are also the main part of the data, accounting for nearly 20% of the total amount. To ensure visual quality, we only collect data from a high-altitude perspective using Google Earth, which accounts for 4.46%. The *Test Seen* data consists of 1800 trajectories uniformly sampled from 11 previously seen UE and 3D GS scenes, and the *Test Unseen* data comprises 1200 trajectories uniformly generated from 3 unseen scenes, *i.e.*, UE-smallcity, 3D GS-sjtu02, and a Los Angeles-like city in GTA V. Detailed data distributions are shown in Appendix H.

5 OpenFly-Agent

In this section, we present OpenFly-Agent, an aerial VLN model that builds upon the OpenVLA [40] baseline, since OpenVLA and aerial VLN share the same pipeline, *i.e.*, taking images and instructions as input and generating actions. Moreover, OpenVLA is trained on 1M data, having strong abilities in instruction-following and reasoning, which is critical for VLN. In contrast, our model takes a sequence of images to indicate the observation history instead of one image in the original OpenVLA. Additionally, to mitigate visual redundancy between adjacent video frames while

Table 1: Comparison results on the test set. ‘Random’ means randomly selecting one action to execute until the ‘stop’ action is chosen. All models are retrained using our dataset.

Method	test-seen				test-unseen			
	NE↓	SR↑	OSR↑	SPL↑	NE↓	SR↑	OSR↑	SPL↑
Random	242m	0.7%	0.8%	0%	301m	0.1%	0.1%	0%
Seq2Seq[6]	291m	0.1%	3.2%	0.6%	291m	0.1%	0.9%	0.6%
CMA[6]	144m	5.7%	30.0%	5.1%	268m	0.7%	6.6%	0.7%
AerialVLN[17]	<u>130m</u>	6.6%	40.8%	<u>7.0%</u>	227m	2.3%	19.8%	2.2%
Navid[16]	142m	9.9%	24.3%	3.9%	231m	4.2%	<u>27.0%</u>	3.5%
NaVila[44]	140m	<u>14.2%</u>	<u>41.7%</u>	6.7%	<u>226m</u>	4.5%	25.1%	2.9%
OpenFly-Agent (Ours)	98m	33.2%	63.5%	22.8%	178m	10.7%	48.9%	13.3%

maintaining key information, two strategies are proposed, *i.e.*, keyframe selection and visual token merging. First, a series of candidate keyframes is selected. Then, these keyframes are merged temporally before and after the vision encoder, resulting in a compact sequence of visual tokens. Finally, the action decoder discretizes the predicted tokens to 6 action types specific to UAVs. Fig. 4 illustrates the architecture of our OpenFly-Agent, with the details of two strategies described below.

5.1 Keyframe Selection

The length of contextual visual tokens is a major challenge for VLMs when processing videos. Many open-source VLMs use uniform frame sampling [41, 42, 43] to reduce calculation, but this strategy is not suitable for aerial VLN, since it may miss frames containing key landmarks. We notice that sudden changes in the UAV’s trajectory are often caused by the observation of landmarks in both our dataset and AerialVLN [17], which can serve as cues to determine keyframes. Therefore, we adopt a heuristic method to select keyframe candidates near the change point of the UAV’s movement.

To further ensure the precision of training data, scene segmentation maps collected in Sec. 3.2 are used on selected frames to detect landmarks. Frames containing landmarks are selected as keyframes, yielding reasonably accurate results. Note that each sudden change of actions, *e.g.*, from ‘Forward’ to ‘Turn Left’, will produce a set of keyframes. Consequently, we obtain several sets of keyframes for a long trajectory.

5.2 Visual Token Merging

To further reduce redundant information in keyframes, we design visual token merging, where the core concept is to recognize the similarity between image tokens. It compares adjacent keyframes to merge similar regions and maintains its simplicity by token compression.

For each set of candidate keyframes obtained in the previous selection process, a visual encoder maps each input image to multiple visual tokens, with each token representing the information of an image patch. Considering the potential inter-frame patch redundancy, we take a strategy that similar tokens in subsequent adjacent frames are periodically merged. Specifically, we select the first frame in a keyframe set as the reference, since it usually contains the crucial observation indicating the time for action transition. Then, we densely calculate the cosine similarities between each pair of visual tokens of the reference image and the subsequent image. Next, we merge the tokens with high similarity by averaging them. The unmerged tokens in the subsequent frame will be discarded. The merging operation is iteratively performed until the entire keyframe set has been traversed. Besides, we maintain a memory bank with a capacity of K images, which follows a first-in-first-out (FIFO) policy to retain the latest keyframes. Since aerial VLN requires UAVs to perform long-distance flights based on instructions, we continue to conduct token compression within each keyframe to reduce the computational burden. The compressed visual tokens are obtained through grid pooling [45]. Notably, we keep the visual tokens of the current frame uncompressed to capture the latest visual observation, as it contains the most important information for action prediction.

6 Experiments

In this section, we first introduce evaluation metrics, and then present the experimental results and ablation studies. The implementation details of the OpenFly-Agent can be found in Appendix I.

6.1 Evaluation Metrics

Four standard metrics in VLN tasks are adopted to evaluate different methods, *i.e.*, navigation error (NE), success rate (SR), oracle success rate (OSR), and success weighted by path length (SPL). NE measures the average deviation between the UAV’s final stopping point and the ground-truth destination. SR calculates the proportion of successful tasks, where a task is considered successful if the UAV stops within 20 m of the target [17]. In OSR, if any point on the trajectory is within 20 m of the target, the task can be considered successful. SPL calculates the success rate weighted by the ratio of the ground-truth path length to the actually-executed path length.

6.2 Quantitative Results

We evaluate the proposed OpenFly-Agent and multiple VLN methods on the test set, with quantitative results listed in Table 1, where Seq2Seq, CMA, and AerialVLN achieve limited success rates. In contrast, Navid [16] and NaVila [44] are two most recent VLN methods, obtaining better results and demonstrating the great potential of VLMs in aerial VLN. Our OpenFly-Agent achieves the best performance for its strong VLM backbone and the proposed strategies, while aerial VLN is an emerging and challenging task, and there is still much room for improvement. The results on the test-unseen split indicate the generalization abilities of these methods. Similarly, our method achieves better performance, exhibiting a certain degree of robustness. However, all methods are significantly degraded, indicating that more powerful models are urgently needed to be developed. **More qualitative results and real-world experiments are shown in Appendix J and K.**

Table 2: Ablation study on the test-seen split. ‘KS’ and ‘VTM’ denote keyframe selection and visual token merging, respectively.

Method	NE↓	SR↑	OSR↑	SPL↑
OpenVLA (baseline)	196m	3.6%	12.4%	1.9%
History + VTM	215m	12.7%	39.6%	6.4%
KS	275m	6.2%	24.1%	5.6%
KS + VTM	98	33.2%	63.5%	22.8%

6.3 Ablation Study

Ablation studies are conducted to evaluate the contribution of the keyframe selection and visual token merging in OpenFly-Agent. Table. 2 shows the results, where OpenVLA [40] is our baseline. Using only the current frame as an observation makes OpenVLA perform poorly in the aerial VLN task. From ‘History + VTM’ we can see that historical frames significantly improve the success rate. The keyframe selection strategy further increases the SR from 12.7% to 18.5%, demonstrating the effectiveness of key observations. Besides, the comparison between ‘KS’ and ‘KS + VTM’ indicates the great effect of our visual token merging strategy.

7 Limitations and Future Work

The proposed OpenFly platform incorporates various rendering engines/techniques to provide high-quality scenes. Specifically, this is the first attempt to use 3D GS reconstructed scenes to support real-to-sim training and testing, while in the reconstruction of large-scale areas, a few visual artifacts are inevitably present. Future work will focus on exploring more effective reconstruction methods to enhance realism in large-scale scenes. Besides, the proposed OpenFly-Agent is built upon the large VLM model architecture, which is not practical for real-time deployment on UAVs. To address this, future research should focus on developing more efficient architectures and quantization techniques.

8 Conclusion

In this work, we present OpenFly, a platform designed for large-scale data collection in aerial Vision-and-Language Navigation (VLN). OpenFly integrates multiple rendering engines and provides an automatic toolchain for data generation, enabling efficient collection of diverse, high-quality aerial VLN data. The resulting large-scale dataset comprises 100k trajectories across 18 distinct scenes, spanning a wide range of altitudes and lengths, which is significantly superior than existing ones. Furthermore, we propose OpenFly-Agent, a keyframe-aware aerial navigation model capable of directly predicting flight actions based on observations and language instructions. Extensive experiments validate the effectiveness of the proposed method, and establish a comprehensive benchmark for future advancements in aerial VLN.

References

- [1] H. Chen, A. Suhr, D. Misra, N. Snavely, and Y. Artzi. TOUCHDOWN: natural language navigation and spatial reasoning in visual street environments. In *IEEE Conference on Computer Vision and Pattern Recognition*, 2019. 2, 3, 17
- [2] Y. Qi, Q. Wu, P. Anderson, X. Wang, W. Y. Wang, C. Shen, and A. van den Hengel. REVERIE: remote embodied visual referring expression in real indoor environments. In *IEEE/CVF Conference on Computer Vision and Pattern Recognition, CVPR*, 2020. 2, 3, 17, 18
- [3] P. Anderson, Q. Wu, D. Teney, J. Bruce, M. Johnson, N. Sünderhauf, I. D. Reid, S. Gould, and A. van den Hengel. Vision-and-language navigation: Interpreting visually-grounded navigation instructions in real environments. In *IEEE Conference on Computer Vision and Pattern Recognition*, 2018. 2, 3, 17, 18
- [4] A. Ku, P. Anderson, R. Patel, E. Ie, and J. Baldridge. Room-across-room: Multilingual vision-and-language navigation with dense spatiotemporal grounding. In *Proceedings of the 2020 Conference on Empirical Methods in Natural Language Processing*, 2020. 2, 3, 17
- [5] J. Thomason, M. Murray, M. Cakmak, and L. Zettlemoyer. Vision-and-dialog navigation. In *3rd Annual Conference on Robot Learning, CoRL 2019, Osaka, Japan, October 30 - November 1, 2019, Proceedings*, volume 100 of *Proceedings of Machine Learning Research*, pages 394–406, 2019. 2, 3, 17
- [6] J. Krantz, E. Wijmans, A. Majumdar, D. Batra, and S. Lee. Beyond the nav-graph: Vision-and-language navigation in continuous environments. In *Computer Vision - ECCV 2020 - 16th European Conference, Glasgow, 2020*. 2, 3, 6, 7, 17
- [7] D. K. Misra, A. Bennett, V. Blukis, E. Niklasson, M. Shatkhin, and Y. Artzi. Mapping instructions to actions in 3d environments with visual goal prediction. In *Proceedings of the 2018 Conference on Empirical Methods in Natural Language Processing, Brussels*, 2018. 2, 3, 17
- [8] Y. Long, W. Cai, H. Wang, G. Zhan, and H. Dong. Instructnav: Zero-shot system for generic instruction navigation in unexplored environment. *arXiv preprint arXiv:2406.04882*, 2024. 2
- [9] K. Chen, J. K. Chen, J. Chuang, M. Vázquez, and S. Savarese. Topological planning with transformers for vision-and-language navigation. In *Proceedings of the IEEE/CVF Conference on Computer Vision and Pattern Recognition*, pages 11276–11286, 2021. 2
- [10] S. Raychaudhuri, S. Wani, S. Patel, U. Jain, and A. X. Chang. Language-aligned way-point (law) supervision for vision-and-language navigation in continuous environments. *arXiv preprint arXiv:2109.15207*, 2021. 2
- [11] G. Georgakis, K. Schmeckpeper, K. Wanchoo, S. Dan, E. Miltsakaki, D. Roth, and K. Daniilidis. Cross-modal map learning for vision and language navigation. In *Proceedings of the IEEE/CVF Conference on Computer Vision and Pattern Recognition*, pages 15460–15470, 2022. 2

- [12] Y. Hong, Z. Wang, Q. Wu, and S. Gould. Bridging the gap between learning in discrete and continuous environments for vision-and-language navigation. In *Proceedings of the IEEE/CVF Conference on Computer Vision and Pattern Recognition*, pages 15439–15449, 2022. 2
- [13] Z. Wang, X. Li, J. Yang, Y. Liu, and S. Jiang. Sim-to-real transfer via 3d feature fields for vision-and-language navigation. *arXiv preprint arXiv:2406.09798*, 2024. 2
- [14] Z. Wang, X. Li, J. Yang, Y. Liu, and S. Jiang. Gridmm: Grid memory map for vision-and-language navigation. In *Proceedings of the IEEE/CVF International Conference on Computer Vision*, pages 15625–15636, 2023. 2
- [15] P. Chen, D. Ji, K. Lin, R. Zeng, T. H. Li, M. Tan, and C. Gan. Weakly-supervised multi-granularity map learning for vision-and-language navigation. *arXiv preprint arXiv:2210.07506*, 2022. 2
- [16] J. Zhang, K. Wang, R. Xu, G. Zhou, Y. Hong, X. Fang, Q. Wu, Z. Zhang, and H. Wang. Navid: Video-based vlm plans the next step for vision-and-language navigation. *Robotics: Science and Systems*, 2024. 2, 4, 7, 8, 19
- [17] S. Liu, H. Zhang, Y. Qi, P. Wang, Y. Zhang, and Q. Wu. Aerialvln: Vision-and-language navigation for uavs. In *IEEE/CVF International Conference on Computer Vision, ICCV 2023, Paris, France, October 1-6, 2023*, pages 15338–15348, 2023. 2, 3, 4, 6, 7, 8, 13, 17, 18, 19
- [18] X. Wang, D. Yang, Z. Wang, H. Kwan, J. Chen, W. Wu, H. Li, Y. Liao, and S. Liu. Towards realistic UAV vision-language navigation: Platform, benchmark, and methodology. *CoRR*, abs/2410.07087, 2024. 2, 3, 4, 17
- [19] A. O’Neill, A. Rehman, and et al. Open x-embodiment: Robotic learning datasets and RT-X models : Open x-embodiment collaboration. In *IEEE International Conference on Robotics and Automation, ICRA 2024, Yokohama, Japan, May 13-17, 2024*, pages 6892–6903, 2024. 2
- [20] Y. Fan, W. X. Chen, T. Jiang, C. ni Zhou, Y. Zhang, and X. Wang. Aerial vision-and-dialog navigation. *ArXiv*, abs/2205.12219, 2022. 3, 17, 18
- [21] J. Lee, T. Miyanishi, S. Kurita, K. Sakamoto, D. Azuma, Y. Matsuo, and N. Inoue. Citynav: Language-goal aerial navigation dataset with geographic information. *CoRR*, abs/2406.14240, 2024. 3, 17, 18
- [22] Q. Hu, B. Yang, S. Khalid, W. Xiao, N. Trigoni, and A. Markham. Sensaturban: Learning semantics from urban-scale photogrammetric point clouds. *Int. J. Comput. Vis.*, 130(2):316–343, 2022. 3
- [23] T. Miyanishi, F. Kitamori, S. Kurita, J. Lee, M. Kawanabe, and N. Inoue. Cityrefer: Geography-aware 3d visual grounding dataset on city-scale point cloud data. In *Advances in Neural Information Processing Systems 36: Annual Conference on Neural Information Processing Systems 2023, NeurIPS 2023, New Orleans, LA, USA, December 10 - 16, 2023*, 2023. 3
- [24] C.-Y. Ma, J. Lu, Z. Wu, G. AlRegib, Z. Kira, R. Socher, and C. Xiong. Self-monitoring navigation agent via auxiliary progress estimation. *arXiv: Artificial Intelligence, arXiv: Artificial Intelligence*, 2019. 3
- [25] X. Wang, Q. Huang, A. Celikyilmaz, J. Gao, D. Shen, Y.-F. Wang, W. Y. Wang, and L. Zhang. Reinforced cross-modal matching and self-supervised imitation learning for vision-language navigation. In *2019 IEEE/CVF Conference on Computer Vision and Pattern Recognition (CVPR)*, 2019. 3
- [26] L. Ke, X. Li, Y. Bisk, A. Holtzman, Z. Gan, J. Liu, J. Gao, Y. Choi, and S. Srinivasa. Tactical rewind: Self-correction via backtracking in vision-and-language navigation. In *2019 IEEE/CVF Conference on Computer Vision and Pattern Recognition (CVPR)*, 2019. 3

- [27] T.-J. Fu, X. E. Wang, M. F. Peterson, S. T. Grafton, M. P. Eckstein, and W. Y. Wang. *Counterfactual Vision-and-Language Navigation via Adversarial Path Sampler*, page 71–86. 2020. 3
- [28] G. Zhou, Y. Hong, and Q. Wu. Navgpt: Explicit reasoning in vision-and-language navigation with large language models. In *Thirty-Eighth AAAI Conference on Artificial Intelligence, AAAI 2024, Thirty-Sixth Conference on Innovative Applications of Artificial Intelligence, IAAI 2024, Fourteenth Symposium on Educational Advances in Artificial Intelligence, EAAI 2014, February 20-27, 2024, Vancouver, Canada*, pages 7641–7649, 2024. 4
- [29] G. Zhou, Y. Hong, Z. Wang, X. E. Wang, and Q. Wu. Navgpt-2: Unleashing navigational reasoning capability for large vision-language models. In *Computer Vision - ECCV 2024 - 18th European Conference, Milan, Italy, September 29-October 4, 2024, Proceedings, Part VII*, volume 15065, pages 260–278, 2024. 4
- [30] J. Chen, B. Lin, R. Xu, Z. Chai, X. Liang, and K. K. Wong. Mapgpt: Map-guided prompting with adaptive path planning for vision-and-language navigation. In *Proceedings of the 62nd Annual Meeting of the Association for Computational Linguistics (Volume 1: Long Papers), ACL 2024, Bangkok, Thailand, August 11-16, 2024*, pages 9796–9810, 2024. 4
- [31] S. Zeng, X. Chang, M. Xie, X. Liu, Y. Bai, Z. Pan, M. Xu, and X. Wei. Futuresight-drive: Thinking visually with spatio-temporal cot for autonomous driving. *arXiv preprint arXiv:2505.17685*, 2025. 4
- [32] S. Raychaudhuri, S. Wani, S. Patel, U. Jain, and A. Chang. Language-aligned waypoint (law) supervision for vision-and-language navigation in continuous environments. *Empirical Methods in Natural Language Processing, Empirical Methods in Natural Language Processing*, 2021. 4
- [33] M. Irshad, N. Mithun, Z. Seymour, H.-P. Chiu, S. Samarasekera, and R. Kumar. Sasra: Semantically-aware spatio-temporal reasoning agent for vision-and-language navigation in continuous environments. *arXiv: Robotics, arXiv: Robotics*, 2021. 4
- [34] J. Krantz, A. Gokaslan, D. Batra, S. Lee, and O. Maksymets. Waypoint models for instruction-guided navigation in continuous environments. In *2021 IEEE/CVF International Conference on Computer Vision (ICCV)*, 2021. 4
- [35] Y. Gao, Z. Wang, L. Jing, D. Wang, X. Li, and B. Zhao. Aerial vision-and-language navigation via semantic-topo-metric representation guided LLM reasoning. *CoRR*, abs/2410.08500, 2024. 4
- [36] B. Kerbl, A. Meuleman, G. Kopanas, M. Wimmer, A. Lanvin, and G. Drettakis. A hierarchical 3d gaussian representation for real-time rendering of very large datasets. *ACM Transactions on Graphics (TOG)*, 43(4):1–15, 2024. 4, 13
- [37] J. L. Schönberger and J.-M. Frahm. Structure-from-motion revisited. In *Conference on Computer Vision and Pattern Recognition (CVPR)*, 2016. 4, 15
- [38] Z. Wang, Y. Su, C. Li, D. Wang, Y. Huang, B. Zhao, and X. Li. Open-vocabulary octree-graph for 3d scene understanding. *CoRR*, abs/2411.16253, 2024. 4, 15
- [39] P. E. Hart, N. J. Nilsson, and B. Raphael. A formal basis for the heuristic determination of minimum cost paths. *IEEE transactions on Systems Science and Cybernetics*, 4(2):100–107, 1968. 5, 16
- [40] M. Kim, K. Pertsch, S. Karamcheti, T. Xiao, A. Balakrishna, S. Nair, R. Rafailov, E. Foster, G. Lam, P. Sanketi, Q. Vuong, T. Kollar, B. Burchfiel, R. Tedrake, D. Sadigh, S. Levine, P. Liang, and C. Finn. Openvla: An open-source vision-language-action model. *arXiv preprint arXiv:2406.09246*, 2024. 6, 8

- [41] S. Buch, C. Eyzaguirre, A. Gaidon, J. Wu, L. Fei-Fei, and J. C. Niebles. Revisiting the” video” in video-language understanding. In *Proceedings of the IEEE/CVF conference on computer vision and pattern recognition*, pages 2917–2927, 2022. 7
- [42] K. Ranasinghe, X. Li, K. Kahatapitiya, and M. S. Ryoo. Understanding long videos in one multimodal language model pass. *arXiv preprint arXiv:2403.16998*, 2024. 7
- [43] X. Wang, Y. Zhang, O. Zohar, and S. Yeung-Levy. Videoagent: Long-form video understanding with large language model as agent. In *European Conference on Computer Vision*, pages 58–76. Springer, 2025. 7
- [44] A.-C. Cheng, Y. Ji, Z. Yang, Z. Gongye, X. Zou, J. Kautz, E. Bıyık, H. Yin, S. Liu, and X. Wang. Navila: Legged robot vision-language-action model for navigation. *arXiv preprint arXiv:2412.04453*, 2024. 7, 8, 19
- [45] Y. Li, C. Wang, and J. Jia. Llama-vid: An image is worth 2 tokens in large language models. In *Computer Vision - ECCV 2024 - 18th European Conference, Milan, Italy, September 29-October 4, 2024, Proceedings, Part XLVI*, volume 15104, pages 323–340, 2024. 7
- [46] Q. Weichao, Z. Fangwei, Z. Yi, Q. Siyuan, X. Zihao, K. Tae, W. Yizhou, and Y. Alan. Unrealcv: Virtual worlds for computer vision. *ACM Multimedia Open Source Software Competition*, 2017. 13
- [47] S. Bonopera, P. Hedman, J. Esnault, S. Prakash, S. Rodriguez, T. Thonat, M. Benadel, G. Chaurasia, J. Philip, and G. Drettakis. sibr: A system for image based rendering, 2020. 14
- [48] S. Bird. Nltk: the natural language toolkit. In *Proceedings of the COLING/ACL 2006 Interactive Presentation Sessions*, pages 69–72, 2006. 17

Appendix

A More Details of Rendering Engines and Data Resources

In this section, more information about the used rendering engines and data resources are detailed, with several high-quality examples illustrated in Fig. 5.

Unreal Engine. UE is a rendering engine capable of providing highly realistic interactive virtual environments. This platform has undergone five iterations, and each version features comprehensive and high-quality digital assets. In UE5, we meticulously select an official sample project named ‘City Sample’, which provides us with a large urban scene covering $25.3km^2$ and a smaller one covering $2.7km^2$. These scenes include a variety of assets such as buildings, streets, traffic lights, vehicles, and pedestrians. Besides, in UE4, we prepare six more high-quality scenes. Specifically, there are two large scenes showcasing the central urban areas of Shanghai and Guangzhou, covering areas of $30.88km^2$ and $58.56km^2$, respectively. The remaining four scenes are selected from AerialVLN [17]. They have smaller areas for totally about $26.64km^2$. These scenes encompass a wide range of architectural styles, including both Chinese and Western influences, as well as classical and modern designs. Additionally, the UE4 engine allows us to make adjustments in scene time to achieve different appearances of scenes under varying lighting conditions.

AirSim is an open-source simulator, which provides highly realistic simulated environments for UAVs and cars. We integrate the AirSim plugin into UE4 to obtain image data easily from the perspective of a UAV.

Since AirSim does not support UE5 and stopped updating in 2022, we use the UnrealCV [46] plugin as an alternative for image acquisition in UE5. To realize a highly efficient data collection in simulated scenes, we modify the UE5 project to a C++ project, integrate the UnrealCV plugin, and package executables for multiple systems like Windows and Linux.

GTA V. GTA V is an open-world game that is frequently used by computer vision researchers due to its highly realistic and dynamic virtual environment. The game features a meticulously crafted cityscape modeled after Los Angeles, encompassing various buildings and locations such as skyscrapers, gas stations, parks, and plazas, along with dynamic traffic flows and changes in lighting and shadows.

Script Hook V is a third-party library with the interface to GTA V’s native script functions. With the help of Script Hook V, we build an efficient and stable interface, which receives the pose information and returns accurate RGB images and lidar data. From the interface, we can control a virtual agent to collect the required data in an arbitrary pose and angle in the game.

Google Earth. Google Earth is a virtual globe software, which builds a 3D earth model by integrating satellite imagery, aerial photographs, and Geographic Information System (GIS) data. From this engine, we select four urban scenes covering a total area of $53.60km^2$, *i.e.*, Berkeley, primarily consisting of traditional neighborhoods; Osaka, which features a mix of skyscrapers and historic buildings; and two areas with numerous landmarks: Washington, D.C., and St. Louis.

Google Earth Studio is a web-based animation and video production tool that allows us to create keyframes and set camera target points on the 2D and 3D maps of Google Earth. Using this functionality, we can quickly generate customized tour videos by selecting specific routes and angles. In order to efficiently plan the route, we develop a function that automatically draws the flight trajectory in Google Earth Studio according to the selected area and predefined photo interval.

3D Gaussian Splatting. As a highly realistic reconstruction method, hierarchical 3D GS [36] employs a hierarchical training and display architecture, making it particularly suitable for rendering large-scale areas. Due to these features, we use this method to reconstruct and render multiple real scenes. We utilize the DJI M30T drone as the data collection device, which offers an automated oblique photography mode, enabling us to capture a large area of real-world data with minimal manpower. Practically, we gathered data from five campuses across three universities, which are East

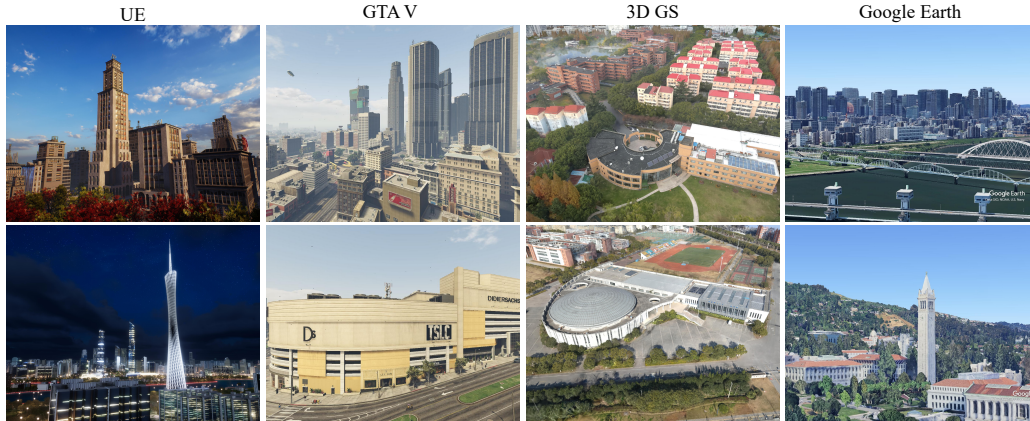


Figure 5: High-quality examples from different rendering engines and techniques, including several large cities such as Shanghai, Guangzhou, Los Angeles, Osaka, and etc., cover an area of over a hundred square kilometers in total. 3D GS provides five large campus scenes, further enhancing the diversity and realism of the data.

Table 3: **Different 3D GS Scenes**

Campus Name	Images	Area
ECUST (Fengxian Campus)	12008	$1.06km^2$
NWPU (Youyi Campus)	4648	$0.8km^2$
NWPU (Changan Campus)	23798	$2.6km^2$
SJTU (Minghang-East Zone)	20934	$1.72km^2$
SJTU (Minghang-West Zone)	9536	$0.95km^2$

China University of Science and Technology, Northwestern Polytechnical University, and Shanghai Jiao Tong University (referred to as ECUST, NWPU, and SJTU). These campus scenes include various types and styles of landmarks, such as libraries, bell towers, waterways, lakes, playgrounds, construction sites, and lawns. The detailed information for the five campuses is presented in Table 3.

SIBR [47] viewers is a rendering tool designed for the 3D GS project, enabling visualization of a scene from arbitrary viewpoints. The tool supports high-frame-rate scene rendering and provides various interactive modes for navigation. Building upon SIBR viewers, we developed an HTTP RESTful API that generates RGB images from arbitrary poses, simulating a UAV’s perspective.

B Details of 3D GS Data Collection

From the UAV’s perspective, choosing the appropriate shooting altitude poses a dilemma, *i.e.*, if the altitude is too low, the sparse point cloud generated during the initialization of the 3D GS reconstruction will be suboptimal, due to insufficient feature point matches between photos. In contrast, if the altitude is too high, the Gaussian reconstruction will result in an overly coarse training of details. After multiple attempts, the data collection plan using the M30T was determined as follows. For large-scale block scenes, oblique photography is performed at approximately twice the average building height using the default parameters of the M30T’s wide-angle camera, with a tilt angle of -45° . For landmark buildings with heights significantly different from the average height, additional targeted data collection is conducted at twice their height. This altitude setting can, to a certain extent, ensure both higher-quality point cloud initialization and Gaussian splatting training.

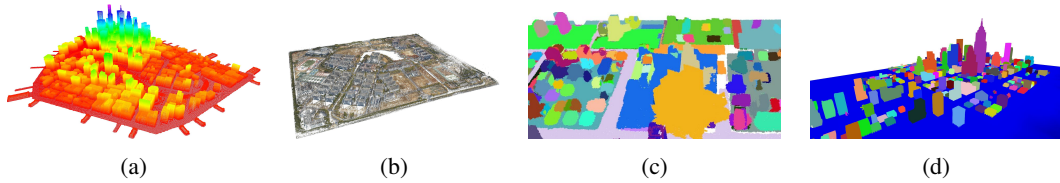


Figure 6: Results of our point cloud acquisition and semantic segmentation. (a) Rasterized sampling point cloud reconstruction. (b) Image-based point cloud reconstruction. (c) Semantic 3D scene segmentation. (d) Point cloud projection and contour extraction.

C Unified Interfaces

For data collection, we integrate all rendering engines and design three unified interfaces, *i.e.*, the agent movement interface, the lidar data acquisition interface, and the image acquisition interface, allowing an agent to move and perceive the environment within any scene.

- **Agent Movement Interface:** We design a *CoorTrans* module, which implements a customized pose transformation matrix and scaling function to unify all coordinate systems into a meter-based FLU (Front-Left-Up) convention. This interface enables precise agent positioning, ensuring consistency and facilitating automatic trajectory generation.
- **Lidar Data Acquisition Interface:** Lidar data is crucial for scene occupancy perception and essential for trajectory generation. Our platform supports different lidar data acquisition methods, including lidar sensor collection, depth map back-projection, and image feature matching. We develop a unified interface to integrate these methods and leverage the proposed *CoorTrans* module to align all data to the same FLU coordinate system.
- **Image Acquisition Interface:** We integrate HTTP RESTful and TCP/IP protocols to form a unified image request interface, allowing image data to be obtained from any location with flexible resolutions and viewpoints.

D Results of Point Cloud Acquisition and Semantic Segmentation

This section presents results regarding the point cloud acquisition and scene semantic segmentation, as shown in Fig. 6.

Point Cloud Acquisition. OpenFly integrates data resources from different rendering engines. In order to obtain point cloud information from different scenes, we provide two point cloud acquisition methods. 1) For UE and GTAV scenes, we provide a tool that utilizes rasterized point cloud sampling and reconstruction to obtain a global point cloud. The results can be seen in Fig. 6a. 2) For 3D GS scenes, we use COLMAP [37] to obtain relatively sparse point data from images, as shown in Fig. 6b. Although the point cloud generated by this method is relatively sparse, it provides sufficient coverage information.

Scene Semantic Segmentation. To meet the requirements of different data resources and different segmentation granularities, our OpenFly offers three methods for obtaining 3D semantic segmentation of scenes. Here, we present results of segmentation methods other than manual annotation. 1) Fig. 6c illustrates the semantic segmentation results based on the off-the-shelf 3D scene understanding method Octree-Graph [38]. This method provides more granular results. 2) The result of semantic segmentation via point cloud projection and contour extraction is shown in Fig. 6d. This method leverages high-precision point clouds to achieve instance segmentation for structures like buildings and trees, which directly contact the ground.

E A Comprehensive Introduction to Automatic Trajectory Generation

Leveraging the point cloud map and segmentation tools, OpenFly offers two methods for trajectory generation for different scenes. 1) Path search based on customized action space: First, a global voxel map M_{global} and a bird’s eye view (BEV) occupancy map M_{bev} are constructed from the scene point cloud. Second, the flight altitude is randomly selected within the user-defined height range, and landmarks that are not lower than the height threshold H_τ are chosen as targets. A starting point is selected within the distance range $[r, R]$ from the landmark, ensuring that it is not occupied in both M_{global} and M_{bev} . Then, a point on the line connecting the starting point and the landmark, which is close to the landmark and unoccupied in M_{bev} , is chosen as the endpoint. Third, A collision-free trajectory from the starting point to the endpoint is generated using the A* [39] pathfinding algorithm, where the granularity of exploration step size and direction can be adjusted according to the action space. Besides, by repeatedly selecting the endpoint as the new starting point, complex trajectories can be generated. Finally, utilizing OpenFly’s interface, images corresponding to the trajectory points can be obtained. 2) Path search based on grid: Google Map data does not allow image retrieval at arbitrary poses in the space. Thus, we rasterize a pre-selected area and collect images from each grid point in all possible orientations. Starting and ending points are chosen within the grid points to generate trajectories. Corresponding images for these trajectory points are then selected from the pre-collected image set.

F Details of Instruction Generation

Except for the instruction generation described in the main paper. The remaining process is mainly divided into two parts: landmark feature extraction and sub-instruction fusion. A simplified prompt to the VLM and the corresponding response are probably like this.

- Get Landmark features.
System Prompt: You are an assistant who is proficient in image recognition. You can accurately identify the object in the picture and its characteristics that are different from the surrounding objects. I will give you the three final images you will see. Please focus on the last image and tell me the features of the target building and reply to me in the form of JSON.
User: The target is the nearest prominent landmark to me. Answer me a dictionary like color:–, feature: –, size: –, type: –.
GPT 4o: color: blue, feature: Steel, glass, size: medium size, type: building.
- Instruction Fusion.
System Prompt: You are an assistant proficient in text processing. You need to help me combine these scattered actions and landmarks into a sentence using words with similar meanings and more appropriate words, making them smooth, fluent, and accurate. If the landmarks of adjacent actions are similar or even identical, please use pronouns to refer to them.
User: Multiple sub-instructions.
GPT 4o: Move forward to a high-rise building with a noticeable logo at the top. Then, slightly turn left and go straight to a futuristic tower with a large spherical structure in the middle.

G Data Quality Control

Data Filter. During data collection, it is inevitable that some damaged or low-quality data will be generated. We clean the data in the following situations. 1) We remove damaged images that are produced in generation or transmission. 2) We find that UAVs sometimes appear to pass through the tree models. Therefore, we exclude the trajectories where the altitude is lower than that of the trees. 3) We believe that extremely short or long trajectories are not conducive to model training. Thus, we remove these trajectories, specifically those with fewer than 2 or more than 150 actions.

Instruction Refinement. A known challenge of instruction generation is VLMs’ hallucinations. During the previous instruction generation process, sometimes the same landmark appears across

Table 4: Comparison of different VLN datasets. N_{traj} : the number of total trajectories. N_{vocab} : vocabulary size. Path Len: the average length of trajectories, measured in meters. Intr Len: the average length of instructions. N_{act} : the average number of actions per trajectory.

Dataset	N_{traj}	N_{vocab}	Path Len.	Intr Len.	Action Space	N_{act}	Environment
R2R [3]	7189	3.1K	10.0	29	graph-based	5	Matterport3D
RxR [4]	13992	7.0K	14.9	129	graph-based	8	Matterport3D
REVERIE [2]	7000	1.6K	10.0	18	graph-based	5	Matterport3D
CVDN [5]	7415	4.4K	25.0	34	graph-based	7	Matterport3D
TouchDown [1]	9326	5.0K	313.9	90	graph-based	35	Google Street View
VLN-CE [6]	4475	4.3K	11.1	19	2 DoF	56	Matterport3D
LANI [7]	6000	2.3K	17.3	57	2 DoF	116	CHALET
ANDH [20]	6269	3.3K	144.7	89	3 DoF	7	xView
AerialVLN [17]	8446	4.5K	661.8	83	4 DoF	204	AirSim + UE
CityNav [21]	32637	6.6K	545	26	4 DoF	-	SensatUrban
OpenUAV [18]	12149	10.8K	255	104	6 DoF	264	AirSim + UE
Ours	100K	15.6K	99.1	59	4 DoF	35	AirSim + UE, GTA V, Google Earth Studio, 3D GS + SIBR viewers

several frames. This results in a VLM generating similar captions for the repeated observations of a landmark, increasing the complexity of the final instruction and introducing ambiguity due to duplication.

To mitigate this challenge, we utilize the NLTK library [48] to simplify the instruction by detecting and merging similar descriptions. Specifically, a syntactic parse tree is first constructed to extract all landmark captions using a rule-based approach. Then, a sentence-transformer model is employed to encode the extracted landmark captions into embedding vectors. Their similarities are computed with dot product, and high-similarity captions are then identified and replaced with referential pronouns (*e.g.*, “it,” “there,” *etc.*). For example, a generated instruction with redundant information is “... make a left turn toward **a medium-sized beige building marked by a signboard reading CHARLIE’S CHOCOLATE**. Continue heading straight, passing **a medium-sized gray building with a prominent rooftop billboard displaying Charlie’s Chocolate** ...”. After simplification, a more concise sentence is obtained, *i.e.*, “... make a left turn toward **a medium-sized beige building marked by a signboard reading CHARLIE’S CHOCOLATE**. Continue heading straight, passing **it** ...”, demonstrating the effectiveness of this post-processing technique.

Manually Check. At the same time, we built a data inspection platform to provide instructions, action sequences, and corresponding images to human examiners. If an instruction describes all the actions and landmarks in a trajectory well, it is considered qualified. We randomly select 3K samples from the entire dataset according to the data distribution. After manually inspecting these samples, we find that they reach a high qualification rate of 91%. There is some ambiguity in the description of some landmarks in the remaining data, making it likely that these landmarks are not easily distinguishable from the surrounding environment. However, the examiners consider this not entirely unacceptable. In summary, most of the generated data feature good quality for the aerial VLN task.

H More Dataset Analyses

Table 4 shows several commonly used statistical information of different VLN datasets, from which we can see that our dataset features a significantly larger number of trajectories and a more extensive vocabulary, as well as greater environmental diversity. In contrast, our average trajectory length and instruction length are relatively short. This is intentional, as we believe short- and medium-range instructions are actually more in line with the usage habits of human users. This might be more beneficial for the aerial VLN field.

Table 5: Linguistic phenomena analysis using randomly selected 25 instructions. p denotes the proportion of instructions showing the phenomenon, and μ represents the average number of times the phenomenon occurs in each instruction.

Phenomenon	R2R[3]		ANDH[20]		AerialVLN[17]		OpenFly		Example in OpenFly
	p	μ	p	μ	p	μ	p	μ	
Reference	100	3.7	92	1.9	100	9.7	100	2.7	...Advance to the large beige and brown building with windows ...
Coreference	32	0.5	8	0.1	68	1.8	52	1.4	...Continue moving forward to reach it ...
Comparison	4	0.0	32	0.4	20	0.2	60	0.7	...Move ahead to the medium-sized beige building ...
Sequencing	16	0.2	8	0.1	68	3.7	64	0.8	...move forward to next large light brown building ...
Allocentric Relation	20	0.2	32	0.4	56	4.6	76	1.0	...black large building featuring a billboard on its rooftop...
Egocentric Relation	80	1.2	32	0.4	100	7.1	100	2.4	... then slightly turn left as you move ahead towards...
Imperative	100	4.0	100	1.1	100	6.9	100	3.6 Proceed slightly straight and turn left
Direction	100	2.8	100	1.4	100	4.6	100	3.8	... turn right and go ahead to ...
Temporal Condition	28	0.4	20	0.2	76	5.6	72	0.9	...Continue straight until you reach ...

Following previous studies [17, 20], we conducted a statistical analysis of the linguistic phenomena using 25 randomly selected instructions and compared the results with other VLN datasets, as detailed in Table 5. The analysis shows that the generated instructions exhibit rich linguistic phenomena such as ‘Reference’ and ‘Comparison’. Notably, our dataset is not the most complex one, since we believe that instructions in VLN tasks should be more aligned with real-life scenarios, rather than emphasizing length and complexity. This cognition is consistent with that of REVERIE [2]. Our instructions avoid overly lengthy and unrealistic expressions to some extent, making them more practical to command UAVs.

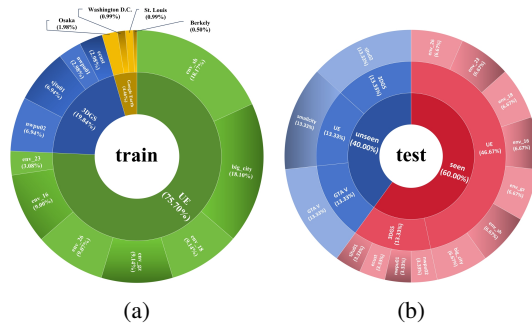


Figure 7: The distribution of the data volume in different scenes under the Train and Test sets. (a) Train set distribution. (b) Test set distribution.

Fig. 7a shows the data distribution of the train set, where 7 UE scenes account for 75.7% of the total 100K data, 4 3D GS scenes account for nearly 20% of the total amount, and Google Earth data accounts for 4.46%. Fig. 7b presents the data distribution of the test set, where the seen data and unseen data account for 60% and 40%, respectively.

I Implementation and Training Details

The proposed OpenFly-Agent is composed of the Dino-SigCLIP (224×224 pixels) as a vision encoder and the pretrained Llama-2 (7B) as a language model. The visual tokens extracted by Dino-SigLIP are aligned to the same dimension as text embeddings using a projection layer, and then fed into the Llama-2 model. The current frame during flight remains 256 tokens and all historical keyframes are compressed into 1 token. The capacity K of the history memory bank is set to 2 in our experiment. For action prediction, the last 256 tokens in the vocabulary are used as special tokens for action representation. Similar to [17, 21], 6 actions for UAVs are defined as {Forward, Turn Left, Turn Right, Move Up, Move Down, Stop} in this work. The units for ‘Move up’ and ‘Move down’ are 3 m, the units for ‘Turn Left’ and ‘Turn Right’ are 30 degrees. ‘Forward’ has three distinct units, namely 3 m, 6 m, and 9 m, respectively.

J Qualitative Experimental Results

Fig. 8 presents a qualitative result in a UE scene, where our OpenFly-Agent successfully navigates to the destination according to the instruction. It presents a powerful capability in perceiving environments and aligning observations with complex instructions. Fig. 9 presents another successful

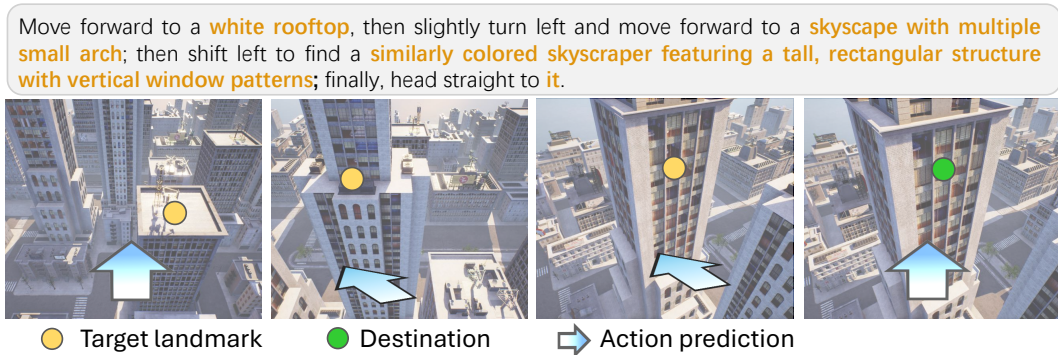


Figure 8: Illustration of an aerial VLN trajectory generated by OpenFly-Agent in a UE scene, which successfully predicts actions following the instruction when encountering landmarks.

Table 6: Results of real-world experiments.

model	SR \uparrow	OSR \uparrow
Navid [16]	13.0%	17.39%
NaVILA [44]	13.0%	21.74%
OpenFly-Agent (Ours)	26.09%	34.78%

Table 7: Performance of OpenFly-Agent trained on different datasets.

dataset	SR \uparrow	OSR \uparrow
AerialVLN [17]	4.3%	13.04%
OpenFly (Ours)	26.09%	34.78%

aerial VLN example in a 3D GS scene. The image style, flight heights, and viewpoints are significantly different from UE’s scenarios. In this case, our OpenFly-Agent exhibits robustness to handle data with great diversity. In addition, Fig. 10 shows two failure cases, where our model sometimes fails to identify the landmark or output actions with proper amplitudes.

K Real-world Experiments

The real-world experiments are conducted in 23 real outdoor scenes, where each scene corresponds to an unseen VLN task created by human operators, and the trajectory lengths range from 50m to 500m. We use a Q250 airframe as a real agent, carrying an NVIDIA Jetson Xavier NX running Ubuntu 18.04 as the onboard computer. All methods run on an external PC communicating with the onboard computer to transfer images and action instructions. Two most recent models, Navid [16] and NaVila [44], are evaluated for comparison. The results are shown in Table 6, where our model achieves the best performance with 26.09% SR and 34.78% OSR, significantly outperforming the comparison methods. This experiment again indicates the superiority of our OpenFly-Agent. Besides, we also trained our model on both our own dataset and the AerialVLN dataset separately. The results are shown in Table 7, where the first row is trained on the AerialVLN dataset (without real-to-sim data), and the second row is trained on our OpenFly dataset. It strongly demonstrates the capability of our data generation method in bridging the sim-to-real gap. A qualitative result is presented in Fig. 11, and a dynamic demo can be found in our supplementary video.



Figure 9: Illustration of aerial VLN trajectories generated by OpenFly-Agent in a 3D GS scene.

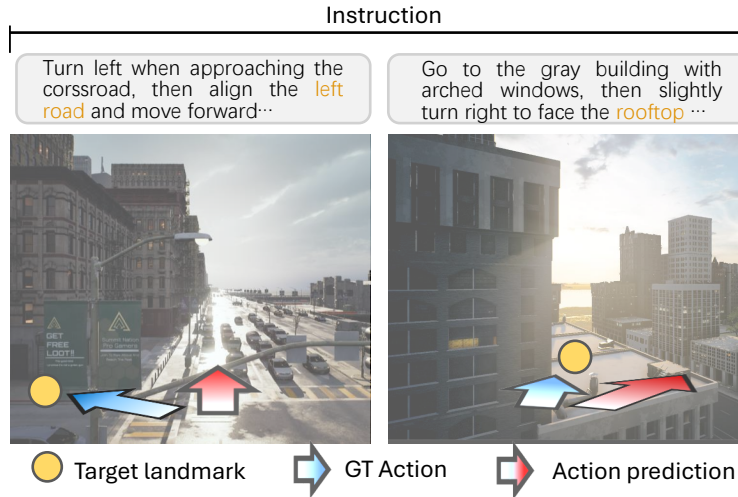


Figure 10: Illustration of failure cases. Sometimes our model may misclassify key landmarks or output wrong actions.



Figure 11: Snapshots of the real-world experiment.